Computation of electron energy loss spectra by an iterative method

Peter Koval[a,b], Mathias Per Ljungberg[a], Dietrich Foerster[c], Daniel Sánchez-Portal[a,b]

[a] *Donostia International Physics Center (DIPC), Paseo Manuel de Lardizabal 4, E-20018 San Sebastián, Spain*
[b] *Centro de Física de Materiales CFM-MPC, Centro Mixto CSIC-UPV/EHU, Paseo Manuel de Lardizabal 5, E-20018 San Sebastián, Spain*
[c] *LOMA, Université de Bordeaux 1, 351 Cours de la Liberation, 33405 Talence, France*

Abstract

A method is presented to compute the dielectric function for extended systems using linear response time-dependent density functional theory. Localized basis functions with finite support are used to expand both eigenstates and response functions. The electron-energy loss function is directly obtained by an iterative Krylov-subspace method. We apply our method to graphene and silicon and compare it to plane-wave based approaches. Finally, we compute electron-energy loss spectrum of C_{60} crystal to demonstrate the merits of the method for molecular crystals, where it will be most competitive.

Keywords: Product basis set, localized functions, extended systems, iterative TDDFT

1. Introduction

The dielectric function (DF) describes the linear response of a solid to external electromagnetic fields [1, 2] and so contains information about experimentally observable quantities like optical absorption spectra and electron energy loss spectra (EELS) [3]. Computing the DF *ab initio* can be efficiently done within time-dependent density function theory (TDDFT). Most approaches in the literature employ plane-wave (PW) basis sets [4–8], although several alternatives that use atomic orbital basis sets have been published [9–11]. PWs offer a natural framework for solids, a stable convergence with the basis set size and diagonal representation of some of the relevant operators. On the other hand, the linear combination of atomic orbitals (LCAO) method allows for an economical description of the electronic structure, especially for molecular solids and open nano structures. In this work, we present a method that consistently uses basis sets of finite support both in the initial density-functional theory (DFT) and in the subsequent TDDFT calculation. We directly obtain the electron-energy loss function by using an iterative method, thus avoiding costly matrix inversions. We start the derivation from widely used PW formulas to make apparent the connections between PW and LCAO in TDDFT.

2. Basic theory

The macroscopic DF is given by a spatial average over the *inverse microscopic* DF [5]

$$\epsilon(\boldsymbol{q},\omega) = 1/\epsilon^{-1}_{\boldsymbol{G}=0,\boldsymbol{G}'=0}(\boldsymbol{q},\omega). \tag{1}$$

The inverse microscopic DF is connected to the interacting response function $\chi_{\boldsymbol{G}''\boldsymbol{G}'}(\boldsymbol{q},\omega)$

$$\epsilon^{-1}_{\boldsymbol{G}\boldsymbol{G}'}(\boldsymbol{q},\omega) = \delta_{\boldsymbol{G}\boldsymbol{G}'} + v_{\boldsymbol{G}\boldsymbol{G}''}\chi_{\boldsymbol{G}''\boldsymbol{G}'}(\boldsymbol{q},\omega), \tag{2}$$

where $v_{\boldsymbol{G}\boldsymbol{G}'} = \frac{4\pi\delta_{\boldsymbol{G}\boldsymbol{G}'}}{|\boldsymbol{G}+\boldsymbol{q}|^2}$ is a Coulomb interaction matrix element between PWs. In the last equation and below in this text we assume summation over repeating indices unless they appear on right-hand side of the equations. The interacting response function satisfies a Petersilka-Gossman-Gross equation [5, 6]

$$\chi_{\boldsymbol{G}\boldsymbol{G}'}(\boldsymbol{q},\omega) = \chi^0_{\boldsymbol{G}\boldsymbol{G}'}(\boldsymbol{q},\omega) + \chi^0_{\boldsymbol{G}\boldsymbol{G}''}(\boldsymbol{q},\omega)K^{\boldsymbol{G}''\boldsymbol{G}'''}(\boldsymbol{q})\chi_{\boldsymbol{G}'''\boldsymbol{G}'}(\boldsymbol{q},\omega). \tag{3}$$

Here the non-interacting response function $\chi^0_{\boldsymbol{G}\boldsymbol{G}'}(\boldsymbol{q},\omega)$ and the TDDFT interaction kernel $K^{\boldsymbol{G}\boldsymbol{G}'}(\boldsymbol{q})$ appear. In this work, we use the so-called RPA approximation $K^{\boldsymbol{G}\boldsymbol{G}'}(\boldsymbol{q}) = v_{\boldsymbol{G}\boldsymbol{G}'}$ for the TDDFT kernel. The non-interacting response function $\chi^0_{\boldsymbol{G}\boldsymbol{G}'}(\boldsymbol{q},\omega)$ has a convenient expression in terms of the Kohn-Sham (KS) eigenstates

$$\chi^0_{\boldsymbol{G}\boldsymbol{G}'}(\boldsymbol{q},\omega) = \frac{1}{N_{\boldsymbol{k}}}\sum_{n,m,\boldsymbol{k}}\frac{(f_{n,\boldsymbol{k}} - f_{m,\boldsymbol{k}+\boldsymbol{q}})U^{\boldsymbol{G}}_{nm}(\boldsymbol{k},\boldsymbol{q})\overline{U}^{\boldsymbol{G}'}_{nm}(\boldsymbol{k},\boldsymbol{q})}{\omega - (E_{m,\boldsymbol{k}+\boldsymbol{q}} - E_{n,\boldsymbol{k}}) + \mathrm{i}\eta}, \tag{4}$$

where the occupation numbers $f_{n,\boldsymbol{k}}$, band energies $E_{n,\boldsymbol{k}}$, broadening constant η and number of $\boldsymbol{k}$-points $N_{\boldsymbol{k}}$ appear. $U^{\boldsymbol{G}}_{nm}(\boldsymbol{k},\boldsymbol{q})$ are matrix elements of PWs in the basis of KS eigenstates $\Psi_{n,\boldsymbol{k}}(\boldsymbol{r})$

$$U^{\boldsymbol{G}}_{nm}(\boldsymbol{k},\boldsymbol{q}) \equiv \int_V \Psi^*_{n,\boldsymbol{k}}(\boldsymbol{r}) \mathrm{e}^{-\mathrm{i}(\boldsymbol{q}+\boldsymbol{G})\boldsymbol{r}} \Psi_{m,\boldsymbol{k}+\boldsymbol{q}}(\boldsymbol{r}) d^3r. \quad (5)$$

3. Method

Using the general expression for the macroscopic DF from section 2, we can establish the connection to electronic structure calculations. We will start with LCAO eigenfunctions and *expand the DF* (2) in a suitable set of *localized basis functions*.

3.1. Localized orbitals in the bulk calculations

We use LCAO in order to expand the eigenstates $\Psi_{n,\boldsymbol{k}}(\boldsymbol{r})$ of Kohn-Sham Hamiltonian

$$\Psi_{n,\boldsymbol{k}}(\boldsymbol{r}) = X^n_a(\boldsymbol{k}) \Phi^a(\boldsymbol{r},\boldsymbol{k}) \quad (6)$$

in terms of Bloch-symmetrized atomic orbitals [1, 2]

$$\Phi^a(\boldsymbol{r},\boldsymbol{k}) = \frac{1}{\sqrt{N}} \sum_{\boldsymbol{R}} \mathrm{e}^{\mathrm{i}\boldsymbol{k}(\boldsymbol{R}+\boldsymbol{R}_a)} f^a(\boldsymbol{r}-\boldsymbol{R}_a-\boldsymbol{R}). \quad (7)$$

Here the number of lattice translations N enters in the normalization constant. (7). The summation in the last equation runs over lattice translations $\boldsymbol{R}$. The local atomic orbitals $f^a(\boldsymbol{r})$ are translated to each periodically repeated copy in the crystal. However, a finite spatial support of localized orbitals $f^a(\boldsymbol{r})$ leaves the possibility for operators to become sparse when the unit cell size exceeds the spatial support. The expansion coefficients in eq. (6) $X^n_a(\boldsymbol{k})$, are determined during a self-consistent Kohn-Sham procedure. We use a DFT package SIESTA [12] for this step.

3.2. Dominant products in the bulk calculations

We want to use functions of finite support not only in DFT, but also in the TDDFT calculation of the DF (1). For this sake, we will construct a set of functions of finite support which is suitable for expanding the response functions (3) and (4). The matrix elements of PWs (5) contain the products of eigenstates. Therefore, it is obvious that the new *product basis* must represent these products accurately. A product of eigenstates translates to a product of Bloch orbitals by virtue of the LCAO expansion (6). Using the definition of the Bloch orbital (7) one gets

$$\overline{\Phi}^a(\boldsymbol{r},\boldsymbol{k})\Phi^b(\boldsymbol{r},\boldsymbol{k}+\boldsymbol{q}) = \frac{1}{N}\sum_{\boldsymbol{R},\boldsymbol{R}'} \mathrm{e}^{-\mathrm{i}\boldsymbol{k}(\boldsymbol{R}_a+\boldsymbol{R})} \mathrm{e}^{\mathrm{i}(\boldsymbol{k}+\boldsymbol{q})(\boldsymbol{R}_b+\boldsymbol{R}')} \times f^a(\boldsymbol{r}-\boldsymbol{R}_a-\boldsymbol{R}) f^b(\boldsymbol{r}-\boldsymbol{R}_b-\boldsymbol{R}'). \quad (8)$$

Due to the finite support of the local orbitals $f^a(\boldsymbol{r})$ and $f^b(\boldsymbol{r})$, the double infinite summation over lattice translations $\boldsymbol{R}$ and $\boldsymbol{R}'$ can be converted to a summation in which only one translation runs infinitely, while the other translation runs only in the neighborhood of the first. For this sake, we introduce a summation over translations $\boldsymbol{S} = \boldsymbol{R}' - \boldsymbol{R}$ that will be finite. Using the super cell translation $\boldsymbol{S}$, one can rewrite eq. (8)

$$\overline{\Phi}^a(\boldsymbol{r},\boldsymbol{k})\Phi^b(\boldsymbol{r},\boldsymbol{k}+\boldsymbol{q}) = \frac{1}{N}\sum_{\boldsymbol{R},\boldsymbol{S}} \mathrm{e}^{-\mathrm{i}\boldsymbol{k}(\boldsymbol{R}_a+\boldsymbol{R})} \mathrm{e}^{\mathrm{i}(\boldsymbol{k}+\boldsymbol{q})(\boldsymbol{R}_b+\boldsymbol{R}+\boldsymbol{S})} \times f^a(\boldsymbol{r}-\boldsymbol{R}_a-\boldsymbol{R}) f^b(\boldsymbol{r}-\boldsymbol{R}_b-\boldsymbol{R}-\boldsymbol{S}). \quad (9)$$

The product of localized function in the last equation is translated infinitely over the lattice. Hence, it is sufficient to find a representation of this product for a zero translation $\boldsymbol{R} = 0$. In our previous work we used a basis of dominant products [13, 14] to expand products of localized functions

$$f^a(\boldsymbol{r}-\boldsymbol{R}_a) f^b(\boldsymbol{r}-\boldsymbol{R}_b-\boldsymbol{S}) = V^{ab\boldsymbol{S}}_\mu F^\mu(\boldsymbol{r}-\boldsymbol{R}_\mu), \quad (10)$$

where expansion coefficients $V^{ab\boldsymbol{S}}_\mu$ and product functions $F^\mu(\boldsymbol{r})$ are found in a diagonalization-based procedure. The product functions $F^\mu(\boldsymbol{r}-\boldsymbol{R}_\mu)$ are centered at the midpoint of the connecting length $\boldsymbol{R}_\mu = (\boldsymbol{R}_a + \boldsymbol{R}_b + \boldsymbol{S})/2$. By inserting the ansatz (10) into eq. (9) one gets

$$\overline{\Phi}^a(\boldsymbol{r},\boldsymbol{k})\Phi^b(\boldsymbol{r},\boldsymbol{k}+\boldsymbol{q}) = V^{ab}_\mu(\boldsymbol{k},\boldsymbol{k}+\boldsymbol{q}) F^\mu(\boldsymbol{r},\boldsymbol{q}), \quad (11)$$

where a Bloch product vertex

$$V^{ab}_\mu(\boldsymbol{k},\boldsymbol{k}+\boldsymbol{q}) = \mathrm{e}^{-\mathrm{i}\boldsymbol{k}\boldsymbol{R}_a} \mathrm{e}^{-\mathrm{i}\boldsymbol{q}\boldsymbol{R}_\mu} \sum_{\boldsymbol{S}} V^{ab\boldsymbol{S}}_\mu \mathrm{e}^{\mathrm{i}(\boldsymbol{k}+\boldsymbol{q})(\boldsymbol{R}_b+\boldsymbol{S})},$$

and a Bloch dominant product function are used

$$F^\mu(\boldsymbol{r},\boldsymbol{q}) = \frac{1}{N}\sum_{\boldsymbol{R}} \mathrm{e}^{\mathrm{i}\boldsymbol{q}(\boldsymbol{R}_\mu+\boldsymbol{R})} F^\mu(\boldsymbol{r}-\boldsymbol{R}_\mu-\boldsymbol{R}). \quad (12)$$

Finally, there is a possibility of using only atom-centered functions in the ansatz (11) instead of using functions centered on the midpoint of two atoms. We will use these atom-centered products in the calculations, although we have to skip a formal derivation here.

3.3. Expansion of response function

The expansion (11) can be used in the non-interacting response function (4). To this end, we insert the product of Bloch orbitals (11) with help of eq. (6) into the matrix element (5)

$$U^{\boldsymbol{G}}_{nm}(\boldsymbol{k},\boldsymbol{q}) = \overline{X}^n_a(\boldsymbol{k}) V^{ab}_\mu(\boldsymbol{k},\boldsymbol{k}+\boldsymbol{q}) X^m_b(\boldsymbol{k}+\boldsymbol{q}) F^\mu_{\boldsymbol{G}}(\boldsymbol{q}), \quad (13)$$

where the Fourier transform of the Bloch function (12) appears

$$F^\mu_{\boldsymbol{G}}(\boldsymbol{q}) = \frac{1}{\sqrt{V_{\text{uc}}}} \mathrm{e}^{-\mathrm{i}\boldsymbol{G}\boldsymbol{R}_\mu} \int_V \mathrm{e}^{-\mathrm{i}(\boldsymbol{q}+\boldsymbol{G})\boldsymbol{r}} F^\mu(\boldsymbol{r}) d^3 r.$$

Here V_{uc} is the volume of unit cell. Using eq. (13), we find for the response function (4)

$$\chi^0_{\boldsymbol{G}\boldsymbol{G}'}(\boldsymbol{q},\omega) = F^\mu_{\boldsymbol{G}}(\boldsymbol{q}) \chi^0_{\mu\nu}(\boldsymbol{q},\omega) \overline{F}^\nu_{\boldsymbol{G}}(\boldsymbol{q}). \quad (14)$$

Here the expansion coefficients $\chi^0_{\mu\nu}(\boldsymbol{q},\omega)$ must be defined by

$$\chi^0_{\mu\nu}(\boldsymbol{q},\omega) = \frac{1}{N_{\boldsymbol{k}}} \sum_{n,m,\boldsymbol{k}} \frac{(f_{n,\boldsymbol{k}} - f_{m,\boldsymbol{k}+\boldsymbol{q}}) U^{nm}_\mu(\boldsymbol{k},\boldsymbol{q}) \overline{U}^{nm}_\nu(\boldsymbol{k},\boldsymbol{q})}{\omega - (E_{m\boldsymbol{k}+\boldsymbol{q}} - E_{n\boldsymbol{k}}) + \mathrm{i}\eta}, \quad (15)$$

where the expansion coefficients $U^{nm}_\mu(\boldsymbol{k},\boldsymbol{q})$ of products of eigenstates in terms of product functions are used

$$U^{nm}_\mu(\boldsymbol{k},\boldsymbol{q}) = \overline{X}^n_a(\boldsymbol{k}) V^{ab}_\mu(\boldsymbol{k},\boldsymbol{k}+\boldsymbol{q}) X^m_b(\boldsymbol{k}+\boldsymbol{q}).$$

Furthermore, for the interacting response function $\chi_{\boldsymbol{G}\boldsymbol{G}'}(\boldsymbol{q},\omega)$ we use an ansatz similar to eq. (14) and rewrite eq. (3) in the basis of Bloch product functions

$$\chi_{\mu\nu}(\boldsymbol{q},\omega) = \chi^0_{\mu\nu}(\boldsymbol{q},\omega) + \chi^0_{\mu\mu'}(\boldsymbol{q},\omega) K^{\mu'\nu'}(\boldsymbol{q}) \chi_{\nu'\nu}(\boldsymbol{q},\omega), \quad (16)$$

where the interaction kernel $K^{\mu\nu}(\boldsymbol{q})$ has to be introduced

$$K^{\mu\nu}(\boldsymbol{q}) = \sum_{\boldsymbol{G}\boldsymbol{G}'} \overline{F}^\mu_{\boldsymbol{G}}(\boldsymbol{q}) K^{\boldsymbol{G}\boldsymbol{G}'}(\boldsymbol{q}) F^\nu_{\boldsymbol{G}'}(\boldsymbol{q}). \quad (17)$$

In the calculations, we only use the Hartree kernel $K^{\boldsymbol{G}\boldsymbol{G}'}(\boldsymbol{q}) = v_{\boldsymbol{G}\boldsymbol{G}'}(\boldsymbol{q})$, although any local or semi-local interaction kernel can be used.

3.4. Iterative computation of dielectric function

Using eqs. (1), (2) with ansatz (14), we get the inverse macroscopic DF in terms of localized functions

$$\epsilon^{-1}(\boldsymbol{q},\omega) = 1 + \frac{4\pi}{q^2} F^\mu_{\boldsymbol{0}}(\boldsymbol{q}) \chi_{\mu\nu}(\boldsymbol{q},\omega) \overline{F}^\nu_{\boldsymbol{0}}(\boldsymbol{q}), \quad (18)$$

where the interacting response function $\chi_{\mu\nu}(\boldsymbol{q},\omega)$ can be determined by solving eq. (16). The solution of the matrix equation is a computationally demanding task. However, if only the DF (18) is needed, then one can avoid the solution of matrix eq. (16). We reformulate the problem in terms of solving of a linear equation

$$(\mathbf{1} - \chi^0 K) X = \chi^0 \overline{F}_{\boldsymbol{0}}$$

and a subsequent calculation of the DF (18) $\epsilon^{-1}(\boldsymbol{q},\omega) = 1 + \frac{4\pi}{q^2} F^\mu_{\boldsymbol{0}}(\boldsymbol{q}) X_\mu(\boldsymbol{q})$. Moreover, applying an *iterative, Krylov subspace scheme* [15] for solving the linear equation, one can significantly reduce the computational cost. The whole problem of computation of the DF will be done in terms of matrix–vector operations, applying $(\mathbf{1} - \chi^0 K)^\nu_\mu$ to vectors z_ν. One can split the matrix–vector operation in two: application of the kernel K to the vector z_ν and subsequent application of response function to the intermediate vector Kz. The kernel (17) is a full matrix. We precompute the kernel before the iterative procedure and apply it to vectors using standard BLAS subroutines. The application of the non-interacting response function (15) to a vector can also be split into several steps. The particular sequence of operations in the computation of $\chi^0_{\mu\nu} z^\nu$ is shown in figure 1. Firstly, we compute the product $V^{cd}_\nu z^\nu$. Sec-

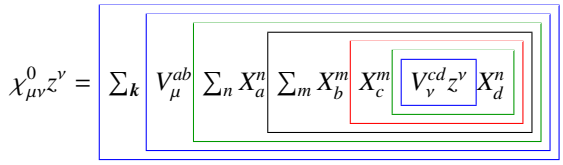

Figure 1: The realized sequence of operations for $\chi^0 \times$ vector product.

ondly, we multiply with the eigenvector X^n_d, etc. Because the vertex coefficients V^{ab}_μ are $\boldsymbol{k}$-dependent, we perform the sum over the Brillouin zone (BZ) in an outer loop and compute products $\chi^0_{\mu\nu} z^\nu$ simultaneously for a set of frequencies $\{\omega\}$. This method reduces the number of operations significantly. The asymptotical computation complexity of the method is $N^3_{\text{a}} N_{\boldsymbol{k}}$, where N_{a} is number of atoms in the unit cell. As iterative solver, we use modified CERFACS subroutines which implement the Generalized Minimal Residue method [16].

4. Results

In the figure 2, we compare the EELS of graphene computed by our iterative method with published calculations [6]. The parameters for this comparison were chosen as in the publication [6]. Namely, the momentum transfer $\boldsymbol{q} = 0.046\text{Å}^{-1}$ in plane in the $\Gamma - \text{M}$ direction, the distance between graphene layers 20Å and

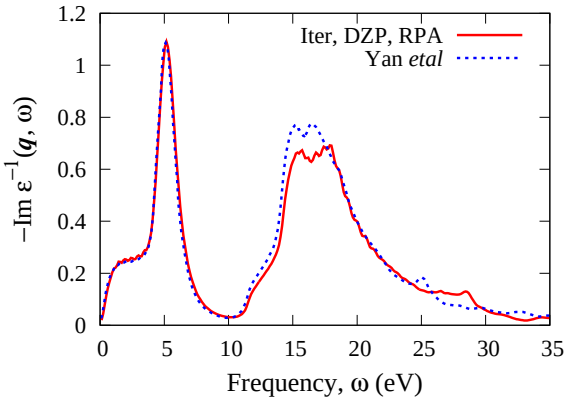

Figure 2: EELS of graphene computed with our iterative method versus a mixed Grid–PW calculation [6].

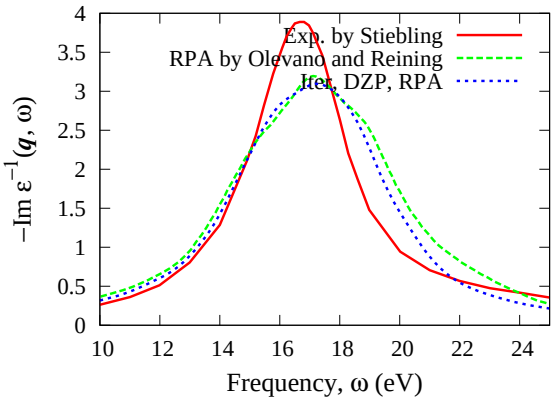

Figure 3: EELS of silicon with computed with our iterative method versus calculation in PW basis [20] and measurements [19].

the sampling of BZ $64 \times 64 \times 1$ were used. The frequency broadening was set to $\eta = 0.24$ eV. In the DFT calculation we used a double zeta polarized (DZP) basis with an energy shift parameter 50 meV, the Perdew–Zunger (LDA) exchange-correlation functional [17] and Troullier–Martins pseudo-potentials [18]. For the computation of the Hartree kernel (17), a set of PWs with an energy cutoff of $E_{\text{cut}} = 200$eV (resulting in 651 PWs) was seen to give converged results and was subsequently used. The number of product basis functions was 138 (69 per atom in the unit cell), which is substantially lower than number of plane waves needed for convergence in this calculation. There are small discrepancies between the calculations. These discrepancies are most probably due to the basis sets used (spatial grid versus DZP basis in our calculation) as well as to the differences in the TDDFT kernel (LDA versus RPA).

The next comparison is shown in the figure 3. We compare our calculation for silicon with measurements [19] and with other independent calculations [20]. The parameters in the DFT calculation were the same as in the graphene example. We chose a small momentum transfer $q = 0.1336\text{Å}^{-1}$, and an energy cutoff $E_{\text{cut}} = 250$eV, which resulted in 339 PWs. The frequency broadening was set to $\eta = 0.6$ eV. The BZ sampling was seen to be converged with $15\times15\times15$ points. The number of product basis functions was 136 (68 per atom in the unit cell), which is again lower than number of PWs needed for convergence (about 250). In figure 3 we see a good agreement between calculations but less satisfactory agreement with experiment. The discrepancies between theory and experiment must be attributed to deficiencies in the LDA functional and the RPA kernel.

The final calculation concerns the solid state of C_{60} fullerenes. The structure and electronic properties of fullerite has been extensively studied in the past [21–26]. It is known that buckminster fullerene crystallizes into one of the cubic lattices [21] and one should expect non-negligible effects on the electronic structure induced by the crystal structure [27].

In this work, we compute EELS for the fcc crystal of C_{60} found by Dorset and McCourt [28]. The structure is a result of direct electron-crystallographic analysis of crystals at room temperature — most relevant for applications in organic electronics. The geometry was taken from an open crystallography database [29] (id 9011073) and converted to SIESTA format by `cif2cell` utility [30]. In the DFT calculation, we used the LDA functional, less extended atomic orbitals (energy shift parameter 200 meV), an electronic temperature of 300 K and a $3 \times 3 \times 3$ BZ sampling. The electronic structure corresponds to a semiconductor with a direct band gap of 0.85 eV. The gap value coincides rather well with other LDA calculation by Benning *etal* [31] (0.98 eV), a recent calculation by Zólyomi *etal* [32] (1.06 eV) and with Troullier and Martins [33] (1.18 eV). The momentum transfer was taken as the small value 0.0039 Bohr^{-1} and the broadening constant was set to 0.6 eV. The BZ sampling was seen to be converged with $3 \times 3 \times 3$ points for the resolution defined by broadening of $\eta = 0.6$ eV. An energy cutoff $E_{\text{cut}} = 200$eV was used to define the set of PWs, which resulted in 4015 PWs. The number of product basis functions was 4140 (69 functions per atom, i.e. the same as in the case of graphene example). The runtime on a 12-core machine with Intel Xeon X5550 processor at 2.67GHz was 10 hours, during which a maximum of 10 GMRES iterations per frequency point was performed. EELS curves computed with 9 and 10 iterations are not distinguish-

able on the plot. In figure 4 we see a comparison of our

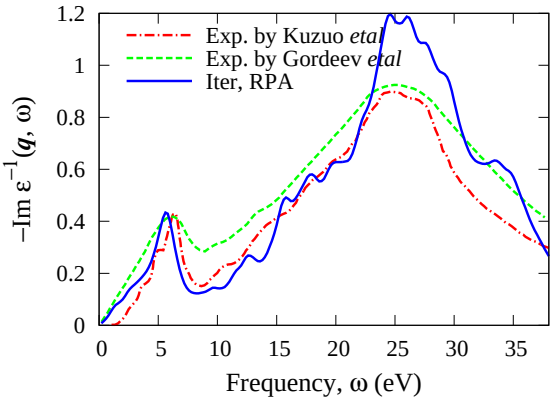

Figure 4: EELS of solid C_{60} computed with our iterative method is compared to measured spectra. Experimental data is taken from [23] and [26].

calculation with experimental data taken from [23] and [26]. As in the case of other carbon-only systems, we find a low-frequency $\pi-\pi^*$ resonance (at about 5.6 eV in the calculation and at about 6.4 eV in the measurements) and $\sigma-\pi$ resonance (at about 25 eV in calculation and measurements). At low resolution, the theoretical result match experimental data rather well. However, a more detailed comparison with higher resolution data in the low frequency range (0–12 eV) is less satisfactory. The discrepancies are probably connected to the accuracy of the DFT functional (determining χ^0) and the TDDFT kernel (RPA in our case). However, the method presented here opens a possibility of practical TDDFT calculations for large systems which would be difficult to achieve with other methods.

Acknowledgments

We acknowledge support from ANR OrgaVolt project. D.S-P. and P.K. acknowledge support from the Basque Departamento de Educación, UPV/EHU (Grant No. IT-366-07), the Spanish Ministerio de Ciencia e Innovación (Grant No. FIS2010-19609-C02-02), the ETORTEK program funded by the Basque Departamento de Industria and the Diputación Foral de Guipuzcoa. D.S-P., P.K. and M.P.L. acknowledge the German DFG through SFB 1083.

[1] C. Kittel, Introduction to Solid State Physics, John Wiley & Sons, Inc., New York, 1986.
[2] R. M. Martin, Electronic Structure: Basic Theory and Practical Methods, Cambridge University Press, Cambridge, 2004.
[3] F. J. García de Abajo, Rev. Mod. Phys. 82 (2010) 209.
[4] A. Marini, *etal*, Comput. Phys. Commun. 180 (2009) 1392.
[5] F. Sottile, *etal*, Int. J. Quant. Chem. 102 (2005) 684.
[6] J. Yan, *etal*, Phys. Rev. B 83 (2011) 245122.
[7] H. Jiang, *etal*, Comput. Phys. Commun. 184 (2013) 348.
[8] X. Gonze, *etal*, Comput. Phys. Commun. 180 (2009) 2582.
[9] A. F. Izmaylov, G. E. Scuseria, Phys. Rev. B 77 (2008) 165131.
[10] M. Rohlfing, *etal*, Phys. Rev. B 52 (1995) 1905.
[11] F. Kootstra, *etal*, J. Chem. Phys. 112 (2000) 6517.
[12] J. M. Soler, *etal*, J. Phys.: Condens. Matter 14 (2002) 2745.
[13] D. Foerster, J. Chem. Phys. 128 (2008) 034108.
[14] D. Foerster, P. Koval, J. Chem. Phys. 131 (2009) 044103.
[15] Y. Saad, Iterative Methods for Sparse Linear Systems, SIAM, 2003.
[16] V. Frayssé, *etal*, ACM Trans. Math. Softw. 35 (2008) 1.
[17] J. P. Perdew, A. Zunger, Phys. Rev. B 23 (1981) 5048.
[18] N. Troullier, J. L. Martins, Phys. Rev. B 43 (1991) 1993.
[19] J. Stiebling, Z. Phys. B 31 (1978) 355.
[20] V. Olevano, L. Reining, Phys. Rev. Lett. 86 (2001) 5962.
[21] W. I. F. David, *etal*, Europhysics Letters 18 (1992) 219.
[22] P. Wochner, *etal*, Phys. Rev. B 55 (1997) 5678.
[23] R. Kuzuo, *etal*, Jpn. J. Appl. Phys. 30 (1991) L1817.
[24] E. Sohmen, J. Fink, Phys. Rev. B 47 (1993) 14532.
[25] R. Kuzuo, *etal*, Phys. Rev. B 49 (1994) 5054.
[26] Y. Gordeev, *etal*, Phys. Solid State 42 (2000) 381.
[27] M. P. Gelfand, J. P. Lu, Phys. Rev. Lett. 68 (1992) 1050.
[28] D. L. Dorset, M. P. McCourt, Acta Cryst. A 50 (1994) 344.
[29] S. Gražulis, *etal*, Nucleic Acids Res. 40 (2012) D420.
[30] B. Torbjörn, Comput. Phys. Commun. 182 (2011) 1183.
[31] P. J. Benning, *etal*, Science 252 (1991) 1417.
[32] V. Zólyomi, *etal*, Phys. Rev. B 78 (2008) 115405.
[33] N. Troullier, J. L. Martins, Phys. Rev. B 46 (1992) 1754.